SEGMENTATION OF ULTRASOUND IMAGES FOR PHLEBOTOMY APPLICATIONS

Dipti Prasad Mukherjee[1] and *Scott T. Acton*[2]
[1]Indian Statistical Institute, Kolkata, [2]University of Virginia, Charlottesville, Virginia, USA

ABSTRACT

A global solution to the enhancement and segmentation of ultrasound images is proposed that is operable in both low contrast and high contrast imaging scenarios. The solution is based on two optimization processes: one that minimizes error with respect to the original image while minimizing the number of edge contours (above the number expected by the known topology), and the second that maximizes edge fidelity. The maximization of edge fidelity is achieved by way of connected filters that operate on connected components of a threshold-decomposed image. To test the algorithm, an application in the ultrasound imaging of human blood vessels is explored. The results show significant improvements (8X to 50X) in a vesselness measure of the segmented vessels as compared to that yielded by a traditional speckle reduction technique and to a diffusion-based technique.

Index Terms—speckle, contrast insensitive, area morphology

1. INTRODUCTION

Reduction of speckle in ultrasound images is a challenging problem, which has been addressed for more than twenty years. As a result a number of speckle reducing filters are in place [1,2]. Modifications to the basic speckle reduction approaches have been proposed where presence of oriented shapes of particular nature are encouraged while smoothing the image in an iterative fashion [3]. Unfortunately, all these approaches use local neighborhood based processing, and no current method uses structural information for speckle reduction. Furthermore, these local approaches are contrast sensitive meaning that they preserve only high contrast regions. One such existing approach to speckle reduction updates partial differential equations in the form of anisotropic diffusion to smooth homogeneous regions while preserving boundaries [2,4,5]. This speckle reducing anisotropic diffusion (SRAD) approach is based on local image features (the local presence or absence of boundaries) and ignorestopology on a global level. Related approaches use local image statistics to remove speckle [6]. Some effort has been made to include global statistics, such as in non-local averaging [7], but these averaging approaches do not consider object shape or topology.

The problem is more complicated for ultrasound images obtained from the hand held devices. Speckle is more salient in images acquired by these portable devices due to limited power and limited computational resources.In this paper we discuss the processing of ultrasound images obtained from hand held devices where the device is placed flat and coplanar with the imaged tissue (in C-mode). The objective of our ultrasound image processing is to retrieve the horizontal cross-sections of a vessel imaged by the ultrasound device so that a 3D visualization of the vessels can be made. Such a 3D segmentation and visualization will enable phlebotomy applications such as needle placement in venipuncture. A typical ultrasound image obtained from the hand held device is shown in Fig. 1(a). Here, the superimposed blue lines are indicative of vessel boundaries.

In contrast to methods that smooth or refrain from smoothing based on gradient magnitude (or some other local measure such as coefficient of variation), the method presented here attempts to retain object structure even in low contrast regions. We believe that the contrast invariance in segmentation is a key contribution of this work. Therefore, our new approach to speckle reduction should give equal importance to the high and low contrast regions however with the overall objective of reducing the number of edges as far as possible. At the same time, the enhanced image should be as faithful as possible to the original image.

One potential solution path is to follow approaches similar to the minimization of total variation [8,9]. In this context, promising results have been obtained in smoothing images with the constraint of simultaneous reduction of number of edges present in the image [10,11]. We utilize a priori information about vessel structure in the form of connected components to produce a contrast-insensitive enhancement and segmentation. In this regard, we have applied area morphology in the form of connected filters [12].

In Section 2, we present the methodology followed by the results and conclusions in Sections 3 and 4, respectively.

2. METHODOLOGY

2.1. Approach to Optimization

With this background, we propose a discrete minimization of $\sum_{p\in I}(I-I_O)^2$ subject to the constraint that $\#\{|\Delta I|^2>0\}\leq k$, where k is the number of desired edge points in the processed image I. The minimization forces the solution$I$ to resemble the observed image I_O in an iterative fashion for every pixel $p\in I$. The edge point strength is defined by $|\Delta I|^2=(\delta I/\delta x)^2+(\delta I/\delta y)^2$.The constraint with an upper bound on edge count serves our primary objective in optimization as stated earlier. The minimization process has no bias towards high or low contrast regions, instead

978-1-4799-2893-4/14/$31.00 ©2014 IEEE

manipulates the resultant number of edges from the image. However we will show that we do not need such an explicit declaration of k in our minimization process. In addition to encourage vessel segmentation, we would like to force only long connected edge points to be present as the vessel boundary. Therefore, at every step we would like to maximize $\sum_{p\in e(C_i)}(|\Delta I|)^2$ which sums the edge strength at every pixel p that belongs to the edge e of the connected component C_i.

The edges of the connected components are the image level lines and can be obtained from the boundary of the binary connected components of image level sets. These image level sets are computed via threshold decomposition of the image, $I_t = (I \geq t)$, where the threshold t ranges typically from minimum to maximum image intensity present in the image in steps of unity or any desired quantization step. Again this process is contrast insensitive providing equal importance to higher or lower contrast region.Therefore, we would like to minimize

$$\sum_{p\in I}(I - I_O)^2 - \sum_{p\in e(C_i)}(|\Delta I|)^2, \#\{|\Delta I|^2 > 0\} \leq k. \qquad (1)$$

Equation (1) has a data fidelity term, $\sum_{p\in I}(I - I_O)^2$, an edge fidelity term $\sum_{p\in e(C_i)}(|\Delta I|)^2$, and a constraint on edge point counts. It is difficult to minimize (1) in a straightforward fashion. The combination of data fidelity and edge fidelity makes the minimization uncertain as no inference about its convergence can be derived. On the other hand the edge point constraint term counts the number of non-zero edges.Combining terms, it is not possible to use standard gradient descent based minimization in such a scenario. However, the entire minimization can be decoupled into multiple steps. First, minimization of the data fidelity term and edge fidelity term can be split into two different steps. The combination of data fidelity term and the remaining constraint part can be expressed as

$$\sum_{p\in I}(I - I_O)^2 + \gamma_1(\#\{|\Delta I|^2 > 0\}), \qquad (2)$$

where, γ_1 is the weight controlling image smoothing in terms of minimization of number of non-zero edges. Therefore, the overall minimization of (1) will continue in two steps:

a) Minimization of (2) followed by
b) Maximization of edge fidelity $\sum_{p\in e(C_i)}(|\Delta I|)^2$.

Minimization of (2) is a well-known splitting problem separating the data fidelity term and the constraint part [10,11,13]. The splitting introduces a common minimizer which can be minimized separately both with the data fidelity part and the constraint part. The common minimizer is effected introducing dummy variables e_x and e_y corresponding to edge gradients along x and y. In the first part of splitting (2), the difference between the actual edge gradients and the dummy variables are minimized along with the minimization of data fidelity term.

$$E_1 = \sum_{p\in I}\left[(I - I_O)^2 + \gamma_2\left(\left((\delta I/\delta x) - e_x\right)^2 + \left((\delta I/\delta y) - e_y\right)^2\right)\right], \qquad (3)$$

with γ_2 being the weight for the common minimizer. The iterative minimization of (3) yields a smoothed image. The convergence of (3), which is the sum of quadratics, is guaranteed. In the second part of splitting (2), the common minimizer is combined with the minimization of the count of the number of non-zero dummy variables (e_x,e_y) corresponding to edge gradients along (*x*,*y*) directions [10].

$$E_2 = \gamma_2\left(\left((\delta I/\delta x) - e_x\right)^2 + \left((\delta I/\delta y) - e_y\right)^2\right) + \gamma_3 n(e_x, e_y). \qquad (4)$$

The function $n(e_x, e_y)$is an indicator function which yields 1 for $\left(|e_x| + |e_y| > 0\right)$, else 0. The importance of $n(e_x, e_y)$ is weighted by γ_3. The energy represented by (4) can be minimized at every image point and after every iteration, the minimization returns a set of (e_x, e_y) values for the image *I*. The minimization of E_2 is guided based on the (e_x, e_y) values. Dividing both sides of (4) by γ_2, if $(e_x, e_y) = (0,0)$, E_2 takes the value of $((\delta I/\delta x)^2 + (\delta I/\delta y)^2)$. If $(e_x, e_y) \neq (0,0)$, E_2 takes the minimum value of (γ_3/γ_2) if $(e_x, e_y) = ((\delta I/\delta x), (\delta I/\delta y))$. Therefore, for a non-zero edge point in an image, if the edge gradient $((\delta I/\delta x)^2 + (\delta I/\delta y)^2)$ is less than some preset value of (γ_3/γ_2), then E_2 has already achieved minima for that edge point. We discuss how (γ_3/γ_2) value is initialized and updated in Section 2.2.

We have implemented the maximization of edge fidelity term, $\sum_{p\in e(C_i)}(|\Delta I|)^2$, using area morphology based filtering. First, we observe that any grayscale image can be represented by threshold decomposition, i.e., a stack of binary images representing regions meeting a threshold. For *K* intensity levels, *K*-1 such binary images are required. An interesting class of filters, called *connected filters*, can be applied to each binary image [14,15]. These filters are capable of only removing or retaining a connected component as a whole. Thus, edges in an image are preserved as edges are simply retained or removed from the image.

There is neither a theoretical convergence result of the algorithm nor a numerical convergence that can be absolutely characterized. However, minimizing the number of non-zero gradient magnitudes in (4) corresponds to the minimization of the L0 semi-norm as done in case of graduated non-convexity based approach [11].

The problem of encouraging longer edges of the connected component representing a homogeneous region in an iterative fashion is treated as the elimination of connected components of the image having less than a specific area [12]. The overall speckle removal algorithm works as follows.

a) The algorithm starts with an initial (γ_3/γ_2) value and it is reduced by a fixed rate at every iteration.
b) If $((\delta I/\delta x)^2 + (\delta I/\delta y)^2) < (\gamma_3/\gamma_2)$, then set $((\delta I/\delta x), (\delta I/\delta y)) = (0,0)$ as E_2 reaches minima at these image sites.
c) Reconstruct image *I* minimizing (3) where some of the edge points of *I* are eliminated in Step (b) above [10].
d) Find connected components in reconstructed *I* for both $I_{t+} = (I \geq t)$ and $I_{t-} = (I < t)$ for t ranging from

minimum to maximum image intensity in steps of unity. Eliminate connected components less than a preset value.

e) The iteration continues till a minimum value of ratio (γ_3/γ_2) is achieved or a single connected component is retained in the segmented image.

The final segmentation is obtained after threshold [16] of the speckle reduced image obtained in Step (e) above.

2.2 Estimation of Parameters

Minimization of (4) is controlled by the ratio (γ_3/γ_2). The initial image contains maximum number of edge points with wide variations in edge strength.Therefore the ratio (γ_3/γ_2) should be set at maximum in order to eliminate most of the undesired edge points while minimizing (4). To initialize the ratio (γ_3/γ_2), we have calculated an edge strength value $\epsilon = ((\delta I/\delta x)^2 + (\delta I/\delta y)^2)$ that separates initial edge strengths into two classes of strong and weak edges with maximum inter-class variance between strong and weak edge classes following [16]. So, using initial (γ_3/γ_2) value, we have ignored all image edge points less than ϵ as in Step (b) above. With the progress of minimization, the inter-class variance between strong and weak edge points is expected to decrease, so as the value of (γ_3/γ_2). Similar to any annealing schedule, in each iteration we have reduced the value of (γ_3/γ_2) by 50% until the ratio (γ_3/γ_2) reached a stationary level. We define that the stationary level is achieved when the difference of two consecutive (γ_3/γ_2) values is less than 0.0001. In the next section we have observed the effect of different reduction rates of (γ_3/γ_2) on the inter-cluster distance, the clusters being the vessel and the background.

The choice of scale for eliminating connected components for Step (c) above is obtained from the histogram of sizes of connected components of the image. This range of scale or size of connected components corresponds to the expected size of the blood vessel that we like to segment. In the following, we present results on ultrasound images of human blood vessels.

3. RESULTS AND DISCUSSIONS

In this section we show the experimental result with two sets of data. Figs. 1(a) and (d) show two 2D *C*-mode images of *in vivo* sample. Figs. 1(b) and (e) are the corresponding images after speckle reduction as detailed in Section 2. Finally, Figs. 1(c) and (f) are the segmented images following [16] on Figs. 1(b) and (e) respectively. The (γ_3/γ_2) ratio value is initialized at 0.72 based on the technique described in Section 2.2. All the connected components less than size τ pixels are removed from the image in every iteration (where τ is the smallest vessel area; in our images τ =1000). A single connected component is obtained when the (γ_3/γ_2) ratio has also achieved stationary value (~25 iterations in these trials). The MATLAB R2011a implementation of the proposed segmentation on 240x400 ultrasound image takes ~29 secs in a 32 GB Dell Precision 3.4 GHz quadcore workstation.

The images of Fig. 1 are the first and the fourth slices within a larger sequence of slices where the vessel is relatively prominent for 3D reconstruction. The stack of all seven 2D images is shown in Fig. 3(a). The stacks are created after placing 2D slices along z-axis. However, for improved visualization, twenty binary 2D slices are interpolated in between every pair of actual 2D slices.

Given the contour points of a segmented vessel (for example, vessels in Figs. 1(c) and (f)) in an actual slice, the corresponding points of the vessel in the next slice are determined based on the minimum Euclidean distance. The twenty intermediate points on a line along z-axis joining the corresponding points of two consecutive 2D slices generate the twenty interpolated slices for visualization. However, for reconstructing the 3D vessel shape, only the seven original 2D slices are stacked to create a 3D binary image. The vessel shape is then reconstructed from the 3D skeleton of the stacked image slices following [17] as shown in Fig. 3(b). For visualization, we have used 1-pixel thick cylinders to reconstruct the 3D vessel. However, the actual dimension in cm can be retrieved from the calibrated z-dimension values of the slices.

Figs. 2(a) and (d) show slices from another set of ultrasound images for which intermediate and segmentation results are shown in Figs. 2(b) and (e) and Figs. 2(c) and (f) respectively. For this image, the initial (γ_3/γ_2) ratio is 0.42 and the number of iterations is 20 while the connected component scale is identical with that of Fig. 1. The corresponding 3D stack image and the 3D reconstructed vessel is shown in Figs. 3(c) and (d) with identical specifications as in Figs. 3(a) and (b) respectively.

To compare the proposed method with the competing approaches, we have shown speckle reduced results of Fig. 1(a) in Figs. 4(a) and (b) using Lee filter [1] and SRAD [2] respectively. The corresponding segmentation results [16] are shown in Figs. 4(d) and (e) respectively. For Lee filter [1] we have used 5x5 masks for averaging with 0.5 as the value of the coefficient of variation. For SRAD [2], we have chosen 400 iterations with 0.02 as the smoothing time step. Clearly, the segmentation results shown in Fig. 1(c) using the proposed approach improve upon those shown in Figs. 4(d) and (e) on a qualitative basis.

In order to compare the performance of the proposed technique quantitatively, we propose *vesselness* measure as extraction of the blood vessel as cylinder as shown in Figs. 3(b) and (d) is the ultimate objective of this proposal. The vesselness measure finds the error in fitting smooth polyline to the segmented inner boundary of the vessels shown in Figs. 1(c), 1(f), 2(c), 2(f) and similar such images. The numerical score of vesselness measure is shown in Table 1.

We have extracted edges of the vessel and used linear regression to fit lines to these edges. The residual sum of fitting error is calculated for all the edge segments and R^2 coefficient of determination is calculated. The R^2 value, vesselness measure, closer to 1 justifies that polyline is better fitted to detected edge so that cylindrical vessel can be reconstructed better. Since, R^2 values are averaged for all the edge segments in the image, our measure penalizes if higher number fragmented edge segments are retrieved after segmentation. The measures in Table 1 show that the proposed method retrieves segment edges from which better vessels can be reconstructed compared to [1] or [2].

To numerically assess the performance of the proposed technique, we have used the result from two sets of phantom images. A typical phantom image and its filtered version using our proposed technique are shown in Figs. 4(c) and (f) respectively. The known diameter for this phantom vessel is 0.5 cm and the vessel length is 1.8 cm. The Table 2 shows results from both *C*-mode normal and compounded beam forming images of phantoms. The second column shows the minimum and maximum retrieved diameters in cm for phantom vessels for 30 slices. The average % of accuracy (over 30 slices) of the retrieved diameter with respect to 0.5 cm ground truth diameter is shown in the third column.

Fig. 5 shows the increasing trend of inter-cluster distance (y-axis) against different decreasing (γ_3/γ_2) values (x-axis) in different iterations for two data sets (Figs. 5(a) and (b) for images of Figs. 1 and 2 respectively). Again, the clusters are vessel and background. Different curves within Figs. 5(a) or (b) represent different annealing rates by which (γ_3/γ_2) value is reduced. In our experiment (γ_3/γ_2) is reduced by 50% at every iteration. Fig. 5 shows that a wide range of annealing rates (in the range of 40-70%) to reduce the (γ_3/γ_2) value is acceptable for our application.

4. CONCLUSIONS

The contribution of this method lies in the ability to enhance and segment ultrasound images despite low contrast boundaries, given knowledge of topology in the form of the number of expected edge contours. The method stands in contrast to methods that rely on local high contrast for enhancement and segmentation. Efficacy in 2-D images shows promise for future extensions to 3-D image volumes.

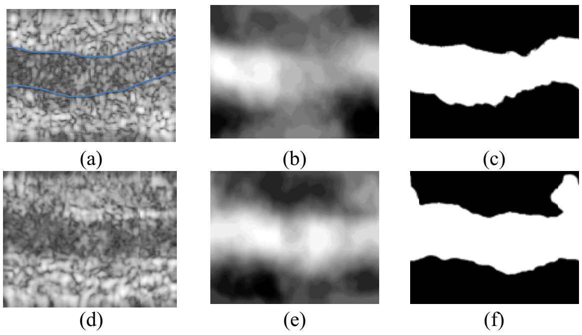

Fig. 1: (a),(d) Original, (b),(e) Speckle removed, (c),(f): Segmented images.

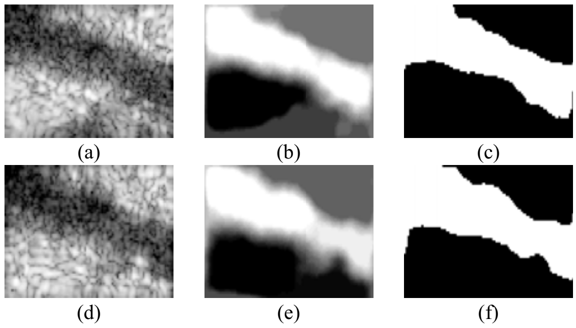

Fig. 2: (a),(d) Original, (b),(e) Speckle removed, (c),(f): Segmented images.

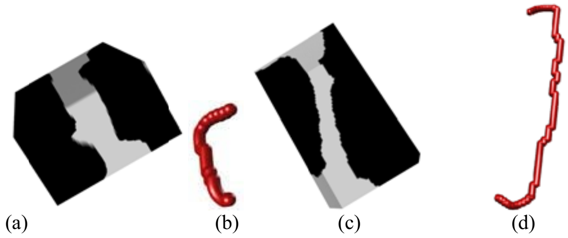

Fig. 3: (a),(c) 3D stack, (b),(d) 3D vessel reconstruction.

Table 1: Vesselness measure.

Data Sets	Lee Filter [1]	SRAD [2]	Proposed
Fig. 1	0.013	0.027	0.176
Fig. 2	0.019	0.223	0.983

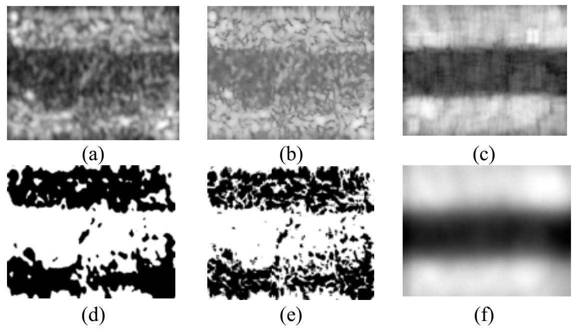

Fig. 4: (a) SRAD on Fig. 1(a), (b) Lee filter on Fig. 1(a), (c) Phantom, (d)-(e): Segmentation on Fig. 4(a)-(b), (f) Proposed method on Fig. 4(c).

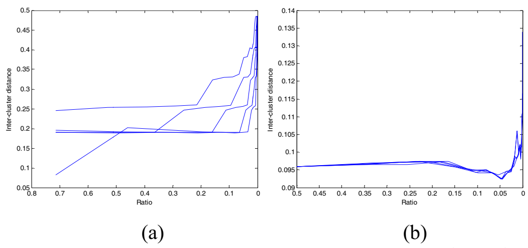

Fig. 5: Change of inter-cluster distance for different(γ_3/γ_2).

Table 2: Numerical assessment of the proposed technique using phantom.

Data set (beam forming)	Vessel size (cm)	Mean (%)
Normal (30 slices)	0.38 to 0.47	80.9
Compounded (30 slices)	0.35 to 0.45	79.3

REFERENCES

[1] J.S. Lee, "Speckle suppression and analysis for synthetic aperture radar," *Opt. Eng.*, 25, 636-643, 1986.

[2] Y. Yu, S.T. Acton, "Speckle reducing anisotropic diffusion," *IEEE Trans. IP*, 11, 1260-1270, 2002.

[3] K. Krissian, C. Westin, R. Kikinis, K.Vosburgh, "Oriented speckle reducing anisotropic diffusion," *IEEE Trans. IP*, May 2007.

[4] P. Perona, J. Malik, "Scale space and edge detection using anisotropic diffusion," *IEEE Trans. PAMI,* 12, 629 – 639, 1990.

[5] S.T. Acton, "Deconvolutional speckle reducing anisotropic diffusion," *Proc. IEEE Int. Conf. on Image Processing*, Genoa, Italy, September 11-14, 2005.

[6] P. Tay, C.D. Garson, S.T. Acton, J.A. Hossack, "Ultrasound despeckling for contrast enhancement," *IEEE Trans. IP*, 19, pp. 1847-1860, 2010.

[7] P. Coupé, P. Hellier, C. Kervrann, C. Barillot,"Nonlocal means-based speckle filtering for ultrasound images,"*IEEE Trans. IP*, 18(10), 2221-2229, 2009.

[8] S. Osher, M. Burger, D. Goldfarb, J.Xu, W. Yin, "An iterative regularization method for total variation-based image restoration,"*Multiscale Modeling & Simulation*,4(2), 460-489, 2005.

[9] L. Vese, S. Osher, "Image denoising and decomposition with total variation minimization and oscillatory functions,"*Journal of Mathematical Imaging and Vision*, *20*(1-2), 7-18, 2004.

[10] L. Xu, C. Lu, Y. Xu, J. Jia, "Image smoothing via *L*0 gradient minimization," *ACM Trans. on Graphics*, 30(6), December 2011.

[11] M. H. Babaie-Zadeh Massoud, C. Jutten, "A fast approach for over complete sparse decomposition based on smoothed l0-norm," *IEEE Trans. SP*, 57(1), 2009.

[12] S.T. Acton, D.P. Mukherjee, "Scalespaceclassification using area morphology," *IEEE Trans. IP.* 9(4), April 2000.

[13] Y. Wang, J. Yang, W. Yin, Y. Zhang, "A new alternating minimization algorithm for total variation image reconstruction,"*SIAM J. Imaging Sciences 1*, 3, 248–272, 2008.

[14] P. Salembier, J. Serra, "Flat zones filtering, connected operators, and filters by reconstruction,"*IEEE Trans. IP*,4(8), 1153-1160, 1995.

[15] P. Salembier, A. Oliveras, L. Garrido, "Antiextensive connected operators for image and sequence processing,"*IEEE Trans. IP*, 7(4), 555-570, 1998.

[16] N Otsu, "A threshold selection method from gray-level histograms," *IEEE Trans. SMC,* 9(1), 62–66, 1979.

[17] Y Zhou, A Toga, "Efficient skeletonization of volumetric objects," *IEEE Trans. VCG*, 5(3), 1999.